Weak impact of mixing on chlorine deactivation during SOLVE/THESEO-2000: Lagrangian modeling (CLaMS) versus ER-2 in situ observations.

Paul Konopka, Jens-Uwe Grooß, Gebhard Günther, Daniel S. McKenna, Rolf Müller
Institute for Stratospheric Chemistry (ICG-1), Jülich, Germany

James W. Elkins
Climate Monitoring and Diagnostics Laboratory, National Oceanic and Atmospheric Administration, Boulder, CO, USA

David Fahey, Peter Popp
Aeronomy Laboratory, National Oceanic and Atmospheric Administration, Boulder, CO, USA

Short title: WEAK IMPACT OF MIXING ON CHLORINE DEACTIVATION DURING SOLVE/THESEO-2000 VERSION FROM May 8, 2002

Abstract. During the second and third segment of the SOLVE campaign in February and March 2000 the Arctic polar vortex had started to be disturbed by planetary waves and upper stratospheric warming events. The perturbations of the vortex were associated with transport of air from low and mid-latitudes into the polar region. Filaments with a lifetime exceeding 2 weeks were generated in regions of strong baroclinicity and peeled off the vortex edge.

The Chemical Lagrangian Model of the Stratosphere (CLaMS) is used for the interpretation of filamentary structures in chemical tracer fields measured on board of the ER-2 during the March flights across the edge of the polar vortex. Both the mixing and the impact of mixing on the chemistry are considered. The isentropic version of CLaMS is initialized on February, 10, at 4 isentropic levels: $\theta = 400$, 425, 450, and 475 K.

A comparison of the measured CH_4/Halon-1211 correlation curves and time series with corresponding CLaMS results obtained for spatial resolution of about 45 km indicates weak mixing between vortex and mid-latitudes air without pronounced anomalous mixing events. Thus, the Arctic vortex in the altitude range 400-475 K was well-isolated during the considered period without significant mass exchange across the vortex edge.

The mixing intensity in CLaMS is controlled by the finite time Lyapunov exponent λ measuring the deformation rate of the horizontal wind and switching on mixing in the flow regions where λ exceeds a critical value λ_c. The CLaMS simulations suggest a temporally and spatially inhomogeneous mixing in the lower stratosphere with a lateral (across the wind) effective diffusion coefficient of the order 10^3 $m^2 s^{-1}$.

The amount of $ClONO_2$ formed due to chemistry induced by mixing of the activated vortex air with NO_x-rich mid-latitude air does not exceed 3%. The impact of mixing on the accumulated ozone loss is less than 1%. The $ClONO_2$-collar observed during the flight on March 11 can be understood as a result of deactivation of ClO_x through the NO_x produced owing to the chemical decomposition of HNO_3 without a significant contribution of mixing with NO_x-rich mid-latitude air.

1. Introduction

Mixing in the stratosphere can be understood as the last step in the scale cascade towards smaller scales driven by the quasi-horizontal stirring of the large scale flow. Stratospheric turbulence is mostly weak and occurs intermittently, as layerwise patches, in regions of strong wind shear and breaking gravity waves [*Nastrom et al.*, 1987]. This is mainly due to the stable stratification of the stratosphere with large bulk Richardson numbers that counteracts vertical motions of the air.

The pre-dominance of chaotic 2d advection in stratospheric transport becomes obvious by the occurrence of laminar structures with typical horizontal and vertical scales of 100 and 1 km, respectively [e.g. *Orsolini et al.*, 1998]. *Reid and Vaughan* [1991] conjecture that such structures originate through differential advection in zones of strong wind shear. Using a linear and horizontal approximation for the stratospheric flow, i.e.

$$(u, v, w) = (s_h x, -s_h y + s_v z, 0) \tag{1}$$

where (x, y, z) are Cartesian coordinates (z - vertical), the horizontal strain s_h and the vertical shear s_v quantify the strength of the sheared zones: Typically, s_v and s_h amount to 10^{-3} s^{-1} [*Dürbeck and Gerz*, 1996] and 10^{-6} s^{-1} [*Tan et al.*, 1998], respectively.

To quantify mixing intensity in the stratosphere, diffusion coefficients based on the Fickian concept of mixing (i.e. mass flux is proportional to the tracer gradient) can be used with vertical diffusivity D_v of the order 0.1 m^2 s^{-1} [*Woodman and Rastogi*, 1984] or smaller [*Balluch and Haynes*, 1997] and horizontal diffusivity D_h of the order 10 m^2 s^{-1} near the tropopause [*Schumann et al.*, 1995].

Inaccurate representation of mixing is potentially an important source of errors in the predictions of photochemical transport models [*Edouard et al.*, 1996; *Searle et al.*, 1998a, b]. Whereas the process of physical mixing occurs in the stratosphere on vertical scales of around 100 m and horizontal scales of the order 10 km [*Balluch and Haynes*, 1997], the concept of effective diffusion can be applied to represent vertical mixing processes in two-dimensional

(e.g. isentropic) models of the stratosphere [*Tan et al.*, 1998]. However, there is a significant uncertainty in the magnitude of the effective diffusivity mainly due to uncertainties in the intensity of the vertical mixing [*Balluch and Haynes*, 1997].

Here, the Chemical Lagrangian Model of the Stratosphere (CLaMS) [*McKenna et al.*, 2001b, a] is applied for the analysis of filamentary structures in both long-lived (CH_4, Halon-1211) and chemically active species ($ClONO_2$, and NO) measured on board of the ER-2 during flights across the filaments near the edge of the polar vortex in March 2000. One of the advantages of CLaMS is that it allows to simulate stratospheric mixing in terms of an adjustable mixing intensity induced by the horizontal deformation of the flow and measured in terms of the finite-time Lyapunov exponent λ. Taking into account that sufficiently large values of λ lead to strong mixing events [*Ngan and Shepherd*, 1999; *Hu and Pierrehumbert*, 2001], we quantify in this paper the intensity of stratospheric mixing in terms of the effective diffusivity and study its influence on the chemical recovery over the course of the second and third segment of the SOLVE campaign in February and March 2000.

The paper is structured as follows: In the next section, we briefly describe the measurements of the chemical species and discuss the meteorological situation during the considered period. Comparing the ER-2 data with CLaMS model results, we quantify in section 3 the magnitude of the effective diffusivity and discuss in section 4 the impact of mixing on the chlorine deactivation within the filaments. Section 5 discusses the results and Section 6 draws the conclusions.

2. Stratospheric meteorology and observations of chemical species

In this paper, the tracer data sampled with ACATS-IV instrument are considered. Among others CH_4 and Halon-1211 time series were measured using the gas chromatography techniques with the precision and accuracy smaller than 1% and 4%, respectively, and with frequency of about 70 s [*Elkins et al.*, 1993; *Romashkin et al.*, 2001]. Further, to study the influence of mixing on the chlorine deactivation, $ClONO_2$ and NO time series are taken into

account. The concentration of $ClONO_2$ is measured with an accuracy and detection limit of $\pm$20% and 10 pptv, respectively, in 35 seconds [*Stimpfle et al.*, 1999]. Detection of NO is accomplished by direct NO/O_3 chemiluminescence at a frequency of 1 Hz [*Fahey et al.*, 1989].

During the second and third segment of the SOLVE campaign in February and March 2000 the lower stratospheric vortex was disturbed by strong planetary waves with zonal wave number 1 and 2 [*Manney and Sabutis*, 2000; *Sabutis and Manney*, 2000]. Interaction with blocking high pressure systems in the upper troposphere and with the Aleutian high led to the generation of long stretched filaments being drawn off the Arctic vortex around the anticyclones. Owing to their large horizontal and vertical extension some of these air masses maintained a strong horizontal PV and tracer gradients for several days. Similar mechanisms led to the generation of filaments of extra-vortex air entering the vortex (see Fig. 1).

Figure 1.

Within the considered period clear signatures of filamentation were measured during two ER-2 flights on March 7 and 11, 2000. The flight on March 7 encountered a filament of extra-vortex air that had entered the vortex three days before over Northern Siberia. The filament was then advected inside the vortex arriving north of Spitsbergen on March 7 when the measurement took place. The filament observed by the ER-2 on March 11 originated from air masses being drawn off the vortex at the end of February. After having been stretched and wrapped around the vortex for almost two weeks, this filament was moving parallel to the vortex edge when it was encountered over Scandinavia. The flight on March 11 crossed the vortex edge and the filament twice on the 450 K isentropic surface.

To study the 3d structure of these filaments, RDF (Reverse-Domain-Filling, [*Sutton et al.*, 1994]) calculations were conducted (see Fig. 2) based on backward trajectory calculations for air parcels (APs) initialized on a uniformly gridded vertical surface (left) or along a flight track (right). For a specific time in the past (here, 15 or 30 days) PV is mapped to the initial parcel locations thereby creating a high-resolution PV field in the domain of interest at the time of observation. The results suggest that some of the small-scale structures observed in the

Figure 2.

CH_4 and Halon-1211 time series near the edge of the Arctic vortex can be interpreted as cuts through sheeted laminar structures of vortex air. The tracer gradients across such structures are a measure of the intensity of the stratospheric mixing. They will be compared in the next section with the corresponding quantities derived from CLaMS model simulations.

Studying the impact of mixing on nonlinear tracer-tracer correlations inside the vortex *Plumb et al.* [2000] suggested that mixing across the vortex edge may lead to anomalous tracer-tracer relationships. An example of nonlinear tracer-tracer relationship is shown in Fig. 3 where CH_4/Halon-1211 correlations derived from all ER-2 flights between January 6, and March 16 are plotted.

Figure 3.

Comparing the data at the beginning (from 6.01 to 3.02, yellow triangles fitted by the blue line) with observations made at the end of this period (from 26.02 to 16.03, pink diamonds fitted by the black line) indicates only a small change of the CH_4/Halon-1211 correlation. Anomalous mixing events [*Waugh et al.*, 1997; *Plumb et al.*, 2000] significantly disrupting the original CH_4/Halon-1211 correlation through long-range (in tracer space) mass exchange between the air parcels (i.e. along dashed lines in Fig. 3) were not observed.

Thus, between the beginning of January and mid of March, tracer transport in the region covered by the ER-2 flights, was dominated by advection rather than mixing indicating a well-isolated vortex. This property of the observed CH_4/Halon-1211 correlation constrains the possible intensity of mixing and, consequently, allows to optimize the mixing parameters in CLaMS. We discuss this issue in the next section.

3. CLaMS tracer simulations

Initialization

Studying stratospheric transport on a timescale of a few weeks we consider CH_4 and Halon-1211 as long-lived atmospheric species. Using the 2d isentropic version of CLaMS [*McKenna et al.*, 2001b], we investigate the transport of these species in the high latitudes

between February 10 and March 15, 2000. Isentropic transport driven by ECMWF winds at four isentropic levels: $\theta = 400$, 425, 450, and 475 K is considered. The isentropic approximation is justified by low total vertical displacement $\Delta\theta < 25$ K due to diabatic effects during the considered period (see Fig. 2, bottom right) calculated using a radiation module [*Zhong and Haigh*, 1995] based on the *Morcrette* [1991] scheme.

At each θ level air parcels (APs) were defined that cover the northern hemisphere with high and low horizontal resolution r_0 north- and southward of 30°N, respectively, r_0 being defined as a mean distance between APs. In the high resolution region, several cases with different spatial resolution are considered with r_0 =30, 45, 60, 100, and 200 km. In the low resolution region, for all cases a constant value r_0 =200 km is assumed.

The initial distribution of CH_4 on February 10 is derived from HALOE and ER-2 data (ACATS) using the PV-tracer correlation shown in Figure 5 in *Grooß et al.* [2001]. The Halon-1211 mixing ratios are initialized by use of the nonlinear relationship derived from ER-2 data observed between January 6, and February 3 (blue curve in Fig. 3).

Pure advection studies (CLaMS without mixing)

Before discussing CLaMS transport where advection and mixing are coupled, it is instructive to consider pure advective transport of CH_4 that is transport based solely on trajectory calculations. The initial positions of APs that characterize a certain spatial resolution r_0 as described above are transported from February, 10 2000 to March 11, 2000, 12 UTC, using isentropic forward trajectories driven by ECMWF winds. For comparison with ER-2 observations during the flight on March 11, we transform the (asynoptic) ER-2 flight track to the synoptic time, March 11, 12 UTC, using forward or backward trajectories and interpolate the results of the simulated CH_4 onto the synoptic flight positions. The results of such a procedure are shown in Fig. 4 where two methods are used: by taking into account the mixing ratio of only the nearest neighbor to the measured AP (green) and by taking into account all next neighbors determined by use of the Delaunay triangulation (red). In the second case a

Figure 4.

weighted interpolation is applied, where a neighbor contributes the more strongly to the result the closer it lies to the considered point. In the first case we approximate the observed mixing ratios by the value of the next neighbor and avoid therefore any kind of numerical diffusion (mixing) due to interpolation.

The comparison of the measured ACATS CH_4 time series (spatial resolution $\approx$ 12 km) with the results of the pure advective transport shows the following features: To resolve the filamentary structure of the vortex edge (dashed regions in Fig. 4) spatial resolution r_0 of the order 100 km or higher is necessary. For all considered values of r_0 the results depend on the method of interpolation. Increasing the spatial resolution r_0 leads to an increase of frequency (not amplitude !) of fluctuations in the simulated time series that is not observed in the ACATS data although their spatial resolution is higher (12 km) than the resolution r_0 of the considered tracer advection studies. This effect can be quantified by comparing the integrated variability of the observed (f_{exp}) and simulated (f_s) CH_4 time series with n data points. In Table 1, the factor $\gamma = \Delta_s/\Delta_{exp}$ with $\Delta_l = \sum_{i=1}^{n} |f_l(t_{i+1}) - f_l(t_i)|$, $l = s, exp$ is determined for the nearest neighbor approximation (green curves in Fig. 4). Note that one expects $\gamma = 1$ if the observed and simulated tracer variability is the same. The γ values in Table 1 increase with the spatial resolution of the model and indicate some “unphysical” tracer fluctuations in pure advection studies with spatial resolution higher then 60 km. The effect of a “too patchy” tracer distribution can also be seen in the 2d isentropic distribution shown in top panels of Fig. 6 where results of a pure advective transport of CH_4 at 450 K are shown.

Table 1.

We interpret these “too patchy” distributions or “unphysical” fluctuations in the simulated time series as a result of missing mixing in the pure advection studies. The next subsection discusses how the CLaMS mixing scheme overcomes this shortcoming using the concept of a dynamically adaptive grid.

CLaMS with variable mixing

Within CLaMS, the mixing of different air masses is determined through a controlled interaction between nearest neighbors identified by Delaunay triangulation. After each advection step Δt mixing between nearest neighbors occurs using the dynamically adaptive grid (for details see *McKenna et al.* [2001b]). Typical values of Δt vary between 6 and 48 hours. For given values of the spatial resolution r_0 and the time step Δt, the intensity of mixing is controlled by a critical Lyapunov exponent λ_c. Mixing in the model occurs only when the finite time Lyapunov exponent λ exceeds a critical value λ_c corresponding to a sufficiently large separation or clustering of the neighboring APs.

Thus, assuming a constant spatial resolution r_0 and a constant time step Δt, mixing intensity can be varied in terms of the critical Lyapunov exponent λ_c. The corresponding (effective) diffusion coefficients $D_\pm(\lambda)$ describe the deformation-dependent mass exchange along $(+)$ and across $(-)$ the wind direction and can be estimated as [*McKenna et al.*, 2001b]:

$$D_\pm(\lambda) = \begin{cases} \frac{r_0^2}{4\Delta t} \exp \pm 2\lambda\Delta t & \lambda \geq \lambda_c \\ 0 & \lambda < \lambda_c. \end{cases} \qquad (2)$$

In the polar regions with a circumpolar flow, $D_\pm(\lambda)$ describes zonal and meridional mixing, respectively. To quantify mixing, we approximate relation (2) for $\lambda \geq \lambda_c$ as $D_\pm^c = D_\pm(\lambda_c)$. The values of $D_\pm^c$ for different configurations of the model parameters r_0, Δt and λ_c are shown in Fig. 5.

Figure 5.

To study the impact of mixing on the distribution of chemically passive and active species we start from the pure advection case described in the previous section and increase the mixing intensity in the model by varying the model parameters r_0, Δt, λ_c and thus the corresponding diffusion coefficients $D_\pm^c$ along the black path in the bottom of Fig. 5. For two model resolution $r_0 = 45$ km (highest CLaMS resolution for tracer transport studies) and 100 km (highest CLaMS resolution with full chemistry, see *Grooß et al.* [2001]), we start at point a) (no mixing), then move to points b) (mixing too small), c), d), and finally reach the point e)

(mixing too high). The significant increase of mixing along this path is due to increase of $D^c_{\perp}$ describing the lateral effective diffusivity and, consequently, smearing out the tracer gradients across the vortex edge. The corresponding values of $D^c_{\perp}$ are shown in Table 2. **Table 2.**

Comparing the simulated time series along the ER-2 track and the CH_4/Halon-1211 correlations with corresponding experimental data, we decide that case c) leads to a best agreement between the model and observations. In Figure 6, CLaMS CH_4 distributions with $r_0 = 45$ km are shown at $\theta = 450$ K for March 7 and for increasing mixing intensities changing from a) to e) along the black path in Fig. 5. **Figure 6.**

To find the most appropriate choice of the mixing parameters we consider now the CH_4/Halon-1211 correlations derived from CLaMS simulations with different mixing intensities. The results calculated for March 11 are plotted in Fig. 7. Here, we take into account all CLaMS APs northward 30°N which are bounded by two envelopes: the outer one (blue solid line) denotes the CH_4/Halon-1211 correlation used for initialization (see Fig. 3) and the inner one (blue dashed line) describing the CLaMS points with anomalous mixing. A polynomial fit through these points is given by the red line. Note that stronger mixing (case e) implicates more compact tracer-tracer correlation. On the other hand, a weak (incomplete) mixing leads to a stronger departure of some mixed APs from the canonical relationship (blue dashed line in case c) [c.f. *Plumb et al.*, 2000]. **Figure 7.**

Now, we compare the mean CLaMS correlations (red curves) with the black curve in Fig. 3 as well as the CLaMS nearest APs along the flight track (red triangles) with the corresponding ACATS observations (black diamonds). As discussed above, a weak change of tracer-tracer correlations was observed between the beginning of February and mid of March (blue and black lines in Fig. 3 and Fig. 7) Consequently, we expect that mean CH_4/Halon-1211 correlations derived from CLaMS simulations show a similar behavior. For the high and low resolution studies the cases c) and b) give the best agreement with the experimental data, respectively.

In addition, the ACATS time series for CH_4 measured on March 11, are compared with

CLaMS results. To allow a proper comparison, we transform the experimental data to a synoptic time (March 11, 12 UCT) using appropriate forward and backward trajectories and compare in Fig. 8 the observed CH_4 values with corresponding CLaMS results using two interpolation methods described in the previous section.

Figure 8.

Considering the simulated tracer time series with increasing mixing (from top to bottom of Fig. 8), two properties should be mentioned: mixing smears out fine structures in the model results that are present in the observations (e.g. filaments in the hatched time segments) and the CLaMS results along the flight track are becoming independent on the kind of interpolation used. Furthermore, CLaMS simulations with higher resolution (lower mixing) reproduce better the tracer gradients at the edges of the filament. Comparing CLaMS with the experimental data in Fig. 8 (i.e. the green or red curves with the observed time series), one can see that although the absolute position of the first filament encounter around 9.50 UTC seems to be well represented in the CLaMS calculations, there is a significant discrepancy between the simulated and observed filament position around 12 UTC. Using UKMO instead of ECMWF winds slightly improves the simulations at this point but makes the comparison for the entire flight significantly worse.

To quantify the agreement between the ACATS observations and CLaMS simulations we compare in terms of the factor γ (see previous section) the spatial variability of the corresponding time series. The results are shown in Table 1 where $\gamma \approx 1$ means that the CLaMS variability of the interpolated time series (nearest neighbor approximation) is comparable with the variability of the experimental data. Based on such analysis, we infer that cases c) and b) for $r_0 = 45$ and $r_0 = 100$ km, respectively, give the best agreement with the observed time series.

4. Impact of mixing on the chemistry

It is an open question to which extent the mixing of activated, ClO_x-rich vortex air with NO_x-rich mid latitude air may cause the deactivation of the stratospheric chlorine and,

consequently, may influence (hinder) chemical ozone depletion. To quantify this effect, full chemistry simulations have been carried out employing the low resolution version of CLaMS ($r_0 = 100$ km) and with different mixing scenarios. The chemical species were initialized as in *Grooß et al.* [2001].

Using mixing parameters introduced in the presented tracer studies (i.e. the time step Δt and the critical Lyapunov exponent λ_c), we show in Fig. 9 the influence of mixing on the formation of an $ClONO_2$-collar and the distribution of NO at the vortex edge. One can see (left side of Fig. 9) that even pure advection study without mixing (top panel) leads to the formation of a $ClONO_2$-collar on the inner side of the vortex edge (black line). This indicates that despite a significant denitrification within the vortex (up to 60% simulated with CLaMS), availably or chemically produced NO_x dominates the formation of $ClONO_2$. We discuss this issue in the next section. **Figure 9.**

If mixing is introduced in the model, it solely smoothes the $ClONO_2$ distribution and slightly increases its total (integral) amount within the vortex (with vortex edge identified by the strongest PV gradient with respect to the equivalent latitude [*Nash et al.*, 1996]). At $\theta = 450$ K mixing increases the total amount of $ClONO_2$ by 3 and 7% for adjusted and excessive mixing, respectively, compared with the pure advection study. Even a too high mixing intensity does not enlarge the $ClONO_2$-collar significantly. It diminishes the $ClONO_2$ gradients across the vortex edge and reduces the structures within the collar region.

Similarly, considering the impact of mixing on the distribution of NO (right side of Fig. 9), a too diffusive transport (bottom panel) smears out the filamentary structure of the vortex edge.

This property of mixing can also be seen if observed time series of chemically active species are compared. On the flight on March 11 the ER-2 crossed the vortex edge twice (Fig. 9). Observed time series of $ClONO_2$ and NO are compared in Fig. 10 with CLaMS results to further investigate the impact of the prescribed mixing intensity in the model. In addition to the weighted interpolation (red curves) discussed in the previous section, we **Figure 10.**

correct the CLaMS time series of NO by taking into account its diurnal variation (violet curves). To this purpose, backward trajectories were calculated from the flight track on March, 11 to a synoptic time on the day before, i.e., March, 10, 12 UTC. Starting at this time, multiple box model calculations were performed that were initialized by an interpolation from CLaMS APs (weighted interpolation). The forward chemical calculations were run up to the time of the measurement. With this method, the effect of the diurnal cycle of photochemically active species is accounted for.

For both types of interpolation the pure advection studies (top panels in Fig. 10) show too much structures compared with the observations. Using the corrected interpolation (violet curve), we can remove systemic discrepancies in the first part of flight between the observed and simulated NO values. On the other side, too much mixing (bottom panels in Fig. 10) completely smears out the filaments near the vortex edge. Similar to the tracer studies, case c) gives the best description of the observed $ClONO_2$ and NO time series.

5. Discussion

The analysis of the CH_4 and Halon-1211 measurements of the ACATS instrument within the altitude range 400 K$< \theta <$ 475 K shows only a small influence of mixing on the tracer distributions within the vortex and near the vortex edge. On the other hand, CLaMS simulations without mixing (i.e. pure advection studies along the isentropic trajectories) carried out with spatial resolution r_0 higher than 100 km produce small scale structures that are not present in the experimental data. Increase of the spatial resolution to $\approx$ 35 km amplifies such “unphysical fluctuations” and indicates missing mixing as their origin.

CLaMS studies including mixing show that only a “small amount” of mixing is necessary to describe the observed CH_4/Halon-1211 correlations and time series. For a given spatial resolution of CLaMS, r_0, the mixing intensity in the model is controlled by the time step Δt after which the dynamically adaptive regridding is applied and the critical Lyapunov coefficient λ_c is switching mixing on in the flow regions with $\lambda > \lambda_c$. Thus, the temporally

and spatially inhomogeneous CLaMS mixing is driven by integral flow deformation over a time step Δt with sufficiently high values of the finite-time Lyapunov exponent λ. Sensitivity studies show that values of the parameters $(\Delta t, \lambda_c)$ leading to a best agreement between CLaMS and experimental data are given by the (black) solid and dashed lines in Fig. 11 for high ($r_0 = 45$ km) and low ($r_0 = 100$ km) cases, respectively. For $\Delta t = 24$ hours, the best choice of the critical Lyapunov exponent is for λ_c between 0.8 and 1.2 day^{-1} with corresponding lateral effective diffusion coefficient $D^c_{\_}$ of the order 10^3 m^{2}s^{-1}.

Figure 11.

It should be emphasized that because of the isentropic approximation used here (in the presented version CLaMS is transporting species on 4 isolated θ-levels) the (numerical) diffusivity $D^c_{\_}$ can only be understood as the effective diffusivity $D_{\rm eff}$ describing the stratospheric mixing in the following sense: During the advection, the CLaMS APs do not leave the isentropic levels and, consequently, describe the mean properties of a stratospheric layer with a certain thickness L_v. Taking into account the unresolved vertical shears on the vertical scales of the order L_v *Haynes and Anglade* [1997] estimated

$$D_{\rm eff} \approx \alpha^2 D_v, \qquad \alpha = \frac{L_h}{L_v} \tag{3}$$

where D_v is the vertical diffusivity and L_h denotes an appropriate horizontal scale. *Balluch and Haynes* [1997] argued that L_v and L_h are vertical and horizontal scales on which the stratosphere is expected to be well mixed and estimated their values as approximately 50 m and 12 km, respectively. The corresponding aspect ratio $\alpha = L_h/L_v$ amounts to about 250. Using relation (3) and published values of the vertical diffusivity *Tan et al.* [1998] estimated that $D_{\rm eff}$ is probably in the range 6×10^0 to 1.25×10^4 m^2 s^{-1}. Taking into account aircraft observations *Waugh et al.* [1997] inferred that $D_{\rm eff}$ is about 5×10^3 m^2 s^{-1}. Mixing in CLaMS generalizes the idea of the (bulk) effective diffusivity $D_{\rm eff}$ to a more realistic inhomogeneous (i.e. driven by spatial and time dependent flow deformation rates) and anisotropic (i.e. dependent on the wind direction) mixing quantified in terms of the spatial resolution r_0, time step Δt, and the critical Lyapunov exponent λ_c.

Investigation of the CH_4/Halon-1211 correlations (Fig. 7) shows that during the considered period anomalous mixing events as described by *Plumb et al.* [2000] are not present either in the observations nor in the corresponding CLaMS simulations along the ER-2 flight track. Nevertheless, because of the limited coverage of the the ER-2 flight and because of the presence of the anomalous mixing events in some CLaMS APs poleward of 30°N (see dashed blue curves in Fig. 7), we cannot exclude that such events occurred in air masses that were not sampled by the ER-2.

Finally, using optimized mixing parameters, we compare in Fig. 12 the observed ACATS CH_4 time series with the corresponding CLaMS results for both flights on March 7 and 11. The investigation of the filaments observed during these flights (hatched areas in Fig. 12) shows that a weak mixing intensity in the model is sufficient to describe the measurements properly. Since only small vertical displacements $\Delta\theta < 25$ K occurred due to diabatic effects during the considered period (see Fig. 2), we do not expect a significant change of our results if diabatic corrections are taken into account. Thus, the transport in the lower stratosphere between mid of February and mid of March, 2000, is clearly dominated by advection rather than by mixing. The comparison between CLaMS simulations based on the ECMWF and UKMO winds shows that the former one matches the observations more properly mainly owing to a higher data frequency (every 6 hours, UKMO: every 24 hours). E.g. the position of the filament observed on March 7 (Fig. 12) is described reasonably well if ECMWF winds are employed whereas using UKMO data the error amounts to $\approx$ 200 km.

Figure 12.

Summarizing, simulations with a weak mixing (see panel c) in Fig. 6) give a better description of the isentropic species distributions than panel e) where overestimated mixing intensity is used. Thus, the stratosphere seems to be much more grainy and spotty than the smooth distributions suggested by Eulerian studies or CLaMS studies with too high mixing intensity.

Studying the chlorine deactivation in the Arctic vortex between beginning of February and mid of March we have shown that the influence of mixing on the chemistry was weak.

The total (integral) amount of $ClONO_2$ formed due to chemistry induced by mixing of the activated vortex air with NO_x-rich mid-latitude air does not exceed 3% of the $ClONO_2$ amount formed without mixing. Even a too high mixing intensity enlarges the amount of mixing-induced $ClONO_2$ only to 7%.

The influence of mixing on the accumulated ozone loss within the vortex is even smaller, i.e. of the order $\approx$ 1%. It should be emphasized that this weak influence of mixing on the chemistry within the polar vortex can be derived only for the considered period and the investigated θ-range. Mixing dominated periods are expected during the vortex formation (fall of 1999) and after mid of March 2000, when the vortex started to decay.

Consequently, the $ClONO_2$-collar observed during the flight on March 11 and successfully reproduced in CLaMS simulations (even without mixing) can be understood as a result of deactivation of ClO_x-rich vortex air with initially present or locally produced NO_x . The main chemical source of NO_x in these APs is the photolytical decomposition of HNO_3 and the reaction of HNO_3 with OH. Thus, in accordance with the study of *Chipperfield et al.* [1997] for the winter 1991/92, it is *in situ* chemical deactivation of ClO_x and not mixing that produces the $ClONO_2$-collar during the considered period.

Using optimized mixing parameters, the CLaMS distributions of $ClONO_2$, ClO_x, HCl and NO_x on March 11, 12 UCT at $\theta = 450$ K are shown in Fig. 13. Note that the inner and outer edges of $ClONO_2$-collar (top left) agree fairly well with the strong gradients of ClO_x (top right) and HCl (bottom left) or NO_x (bottom right), respectively. Thus, the outer edge of $ClONO_2$-collar is defined by the area of ClO_x-activation, i.e. outside of this edge ClO_x was not formed. Air masses bounded by this edge are vortex air masses; the boundary itself can be approximated by the vortex edge identified by the strongest PV gradient with respect to the equivalent latitude [*Nash et al.*, 1996] (black line in Fig. 13). The inner edge of $ClONO_2$-collar is determined by the vortex core where strong denoxification through the formation of HNO_3 occurred. The formation of $ClONO_2$ within this region is deleted through the presence of PSCs leading to a re-activation of ClO_x. Consequently, strong $ClONO_2$ gradients across the

Figure 13.

inner edge can be observed. The mixing ratios within $ClONO_2$-collar depend on the degree of ClO_x-activation experienced by the APs in the past (complete activation corresponds to high $ClONO_2$ -values).

6. Conclusions

The isentropic version of the chemistry transport model CLaMS was used for the interpretation of ER-2 tracer measurements obtained during the second and third segment of the SOLVE campaign in February and March 2000. In particular, the intensity of mixing between the vortex and mid-latitude air masses near the vortex edge and its impact on the chemistry were studied.

A comparison of the measured CH_4/Halon-1211 correlation curves and time series with corresponding CLaMS results indicates weak mixing between vortex and mid-latitudes air without pronounced anomalous mixing events. Thus, the Arctic vortex in the θ-range between 400-475 K was well-isolated during the considered period without significant mass exchange across the vortex edge.

The CLaMS simulations show the best agreement with tracer observations if the lateral (across the wind) effective diffusion coefficient is of the order 10^3 m^2s^{-1}.

The amount of $ClONO_2$ formed due to chemistry induced by mixing of the activated vortex air with NO_x-rich mid-latitude air does not exceed 3%. The influence of mixing on the accumulated ozone loss is even smaller than $\approx$ 1%. The $ClONO_2$-collar observed during the flight on March 11 can be understood as a result of deactivation of ClO_x through the chemical production of NO_x from HNO_3 without significant contribution of mixing with NO_x-rich mid-latitude air.

Acknowledgments.

We are grateful for the contributions of K. Shine, J. Haigh and W. Zhong for providing us with radiation codes. We thank R. Stimpfle for providing us with $ClONO_2$ data. The European Centre

for Medium-Range Weather Forecasts (ECMWF) and the United Kingdom Meteorological Office (UKMO) are acknowledged for meteorological data support. The authors thank Jürgen Ankenbrand and Nicole Thomas for their programming support. This work was funded by the European Union under the contract number EVK2-1999-00311 (EU THESEO 2000) and EVK2-CT-1999-000049 (SAMMOA).

References

Balluch, M. G., and P. H. Haynes, Quantification of lower stratospheric mixing processes using aircraft data, *J. Geophys. Res.*, *102*, 23487–23504, 1997.

Chipperfield, M. P., E. R. Lutman, J. A. Kettleborough, and J. A. Pyle, Model studies of chlorine deactivation and formation of $ClONO_2$ collar in the Arctic polar vortex, *J. Geophys. Res.*, *102*, 1467–1478, 1997.

Dürbeck, T., and T. Gerz, Dispersion of aircraft exhausts in the free atmosphere, *J. Geophys. Res.*, pp. 26007–26015, 1996.

Edouard, S., B. Legras, F. Lefèvre, and R. Eymard, The effect of small-scale inhomogeneities on ozone depletion in the Arctic, *Nature*, *384*, 444–447, 1996.

Elkins, J. W., T. M. Thompson, T. H. Swanson, J. H. Butler, B. D. Hall, S. O. Cummings, D. A. Fisher, and A. G. Raffo, Decrease in the growth rates of atmospheric chlorofluorocarbon-11 and chlorofluorocarbon-12, *Nature*, *364*, 780–783, 1993.

Fahey, D. W., K. K. Kelly, G. V. Ferry, L. R. Poole, J. C. Wilson, D. M. Murphy, M. Loewenstein, and K. R. Chan, In situ measurements of total reactive nitrogen, total water, and aerosol in a polar stratospheric cloud in the Antarctic, *J. Geophys. Res.*, *94*, 11299–11315, 1989.

Grooß, J.-U., et al., Simulation of ozone depletion in spring 2000 with the Chemical Lagrangian Model of the Stratosphere (CLaMS), *J. Geophys. Res.*, 2001, accepted.

Haynes, P., and J. Anglade, The vertical scale cascade in atmospheric tracers due to large-scale differential advection, *J. Atmos. Sci.*, *54*, 1121–1136, 1997.

Hu, Y., and R. T. Pierrehumbert, The advection-diffusion problem for stratospheric flow. Part I: Concentration probability distribution function, *J. Atmos. Sci.*, *57*, 1493–1510, 2001.

Manney, G. L., and J. L. Sabutis, Development of the polar vortex in the 1999-2000 Arctic winter stratosphere, *Geophys. Res. Lett.*, *27*, 2589–2592, 2000.

McKenna, D. S., J.-U. Grooß, G. Günther, P. Konopka, R. Müller, and G. Carver, A new Chemical Lagrangian Model of the Stratosphere (CLaMS): Part II Formulation of chemistry-scheme and initialisation, *J. Geophys. Res.*, 2001a, in press.

McKenna, D. S., P. Konopka, J.-U. Grooß, G. Günther, R. Müller, R. Spang, D. Offermann, and Y. Orsolini, A new Chemical Lagrangian Model of the Stratosphere (CLaMS): Part I Formulation of advection and mixing, *J. Geophys. Res.*, 2001b, in press.

Morcrette, J.-J., Radiation and cloud radiative properties in the European Centre for Medium-Range Weather Forecasts forecasting system, *J. Geophys. Res.*, *96*(D5), 9121–9132, 1991.

Nash, E. R., P. A. Newman, J. E. Rosenfield, and M. R. Schoeberl, An objective determination of the polar vortex using Ertel's potential vorticity, *J. Geophys. Res.*, *101*, 9471–9478, 1996.

Nastrom, G. D., D. C. Fritts, and K. S. Gage, An investigation of terrain effects on the mesoscale spectrum of atmospheric motions, *J. Atmos. Sci.*, *44*, 3087–3096, 1987.

Ngan, K., and T. G. Shepherd, A closer look at chaotic advection in the stratosphere. Part I: Geometric structure, *J. Atmos. Sci.*, *56*, 4134–4152, 1999.

Orsolini, Y. J., G. L. Manney, A. Angel, J. Ovarlez, C. Claud, and L. Coy, Layering in stratospheric profiles of long-lived trace species: Balloon-borne observations and modeling, *J. Geophys. Res.*, *103*, 5815–5825, 1998.

Plumb, R. A., D. W. Waugh, and M. P. Chipperfield, The effect of mixing on tracer relationships in the polar vortices, *J. Geophys. Res.*, *105*, 10047–10062, 2000.

Reid, S. J., and G. Vaughan, Lamination in ozone profiles in the lower stratosphere, *Quart. J. R. Meteorol. Soc.*, *117*, 825–844, 1991.

Romashkin, P. A., D. F. Hurst, J. W. Elkins, G. S. Dutton, D. W. Fahey, R. E. Dunn, F. L. Moore, R. C. Myers, and B. D. Hall, In situ measurements of long-lived trace gases in the lower stratosphere by gas chromatography, *Journal of Atmospheric and Oceanic Technology*, 2001, in press.

Sabutis, J. L., and G. L. Manney, Wave propagation in the 1999-2000 Arctic early winter stratosphere, *Geophys. Res. Lett.*, *27*, 3205–3208, 2000.

Schumann, U., P. Konopka, R. Baumann, R. Busen, T. Gerz, H. Schlager, P. Schulte, and H. Volkert, Estimation of diffusion parameters of aircraft exhaust plumes near the tropopause from nitric oxide and turbulence measurements, *J. Geophys. Res.*, *100*, 14,147–14,162, 1995.

Searle, K. R., M. P. Chipperfield, S. Bekki, and J. A. Pyle, The impact of spatial averaging on calculated polar ozone loss: I. Model experiments, *J. Geophys. Res.*, *103*, 25397–25408, 1998a.

Searle, K. R., M. P. Chipperfield, S. Bekki, and J. A. Pyle, The impact of spatial averaging on calculated polar ozone loss: II. Theoretical analysis, *J. Geophys. Res.*, *103*, 25409–25416, 1998b.

Stimpfle, R. M., et al., The coupling of $ClONO_2$, ClO and NO_2 in the lower stratosphere from in situ observations using the NASA ER-2 aircraft, *J. Geophys Res*, *104*, 26705–26714, 1999.

Sutton, R. T., H. Maclean, R. Swinbank, A. O'Neill, and F. W. Taylor, High-resolution stratospheric tracer fields estimated from satellite observations using Lagrangian trajectory calculations, *J. Atmos. Sci.*, *51*, 2995–3005, 1994.

Tan, D. G. H., P. H. Haynes, A. R. MacKenzie, and J. A. Pyle, Effects of fluid-dynamical stirring and mixing on the deactivation of stratospheric chlorine, *J. Geophys. Res.*, *103*, 1585–1605, 1998.

Waugh, D. W., et al., Mixing of polar vortex air into middle latitudes as revealed by tracer-tracer scatterplots, *J. Geophys. Res.*, *102*, 13119–13134, 1997.

Woodman, R. F., and P. K. Rastogi, Evaluation of effective eddy diffusivity coefficients using radar observations of turbulence in the stratosphere, *Geophys. Res. Lett.*, *211*, 243–246, 1984.

Zhong, W., and J. D. Haigh, Improved broadband emissivity parameterization for water vapor cooling rate calculations, *J. Atmos. Sci.*, *52*(1), 124–138, 1995.

P. Konopka, J.-U. Grooß, G. Günther, D. S. McKenna, R. Müller, Forschungszentrum Jülich, Institute for Stratospheric Chemistry (ICG-1), 52425 Jlich, Germany (e-mail: p.konopka@fz-juelich.de).

J.W. Elkins, Climate Monitoring and Diagnostics Laboratory, National Oceanic and Atmospheric Administration, Boulder, CO, USA (e-mail: jelkins@cmdl.noaa.gov)

D. Fahey, P. Popp, Aeronomy Laboratory, National Oceanic and Atmospheric Administration, Boulder, CO, USA (e-mail: ppopp@al.noaa.gov)

Received _____

Version from May 8, 2002

Figure Captions

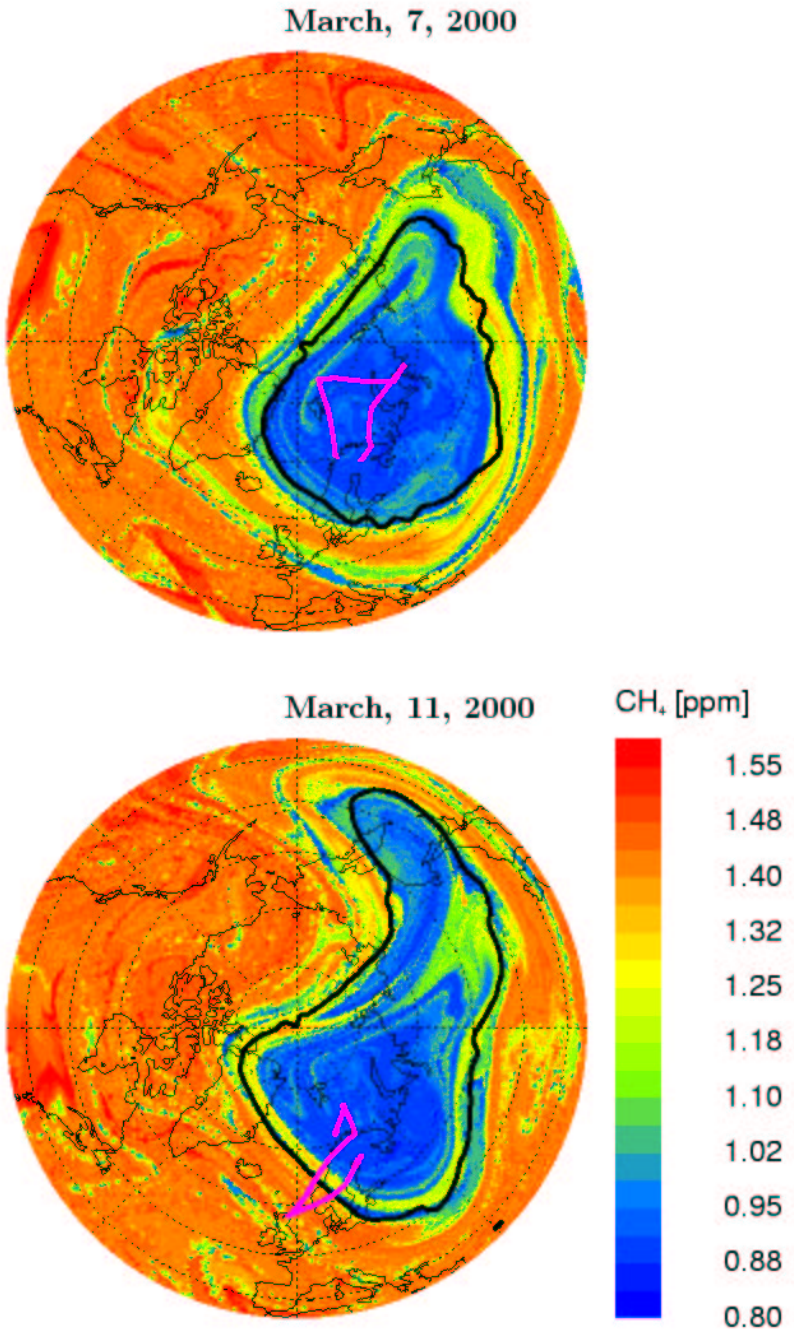

Figure 1. ClaMS distribution of CH_4 in $\theta = 450$ K on March 7 (top) and March 11 (bottom) together with the ER-2 flight track transformed to the synoptic time 12 UCT. For the calculation the optimized mixing intensity was used (see text). On March 7 the ER-2 touched near Spitzbergen a filament of extra-vortex air whereas on March 11 a stretched filament of vortex air was crossed twice at the vortex edge (black line) over Scandinavia.

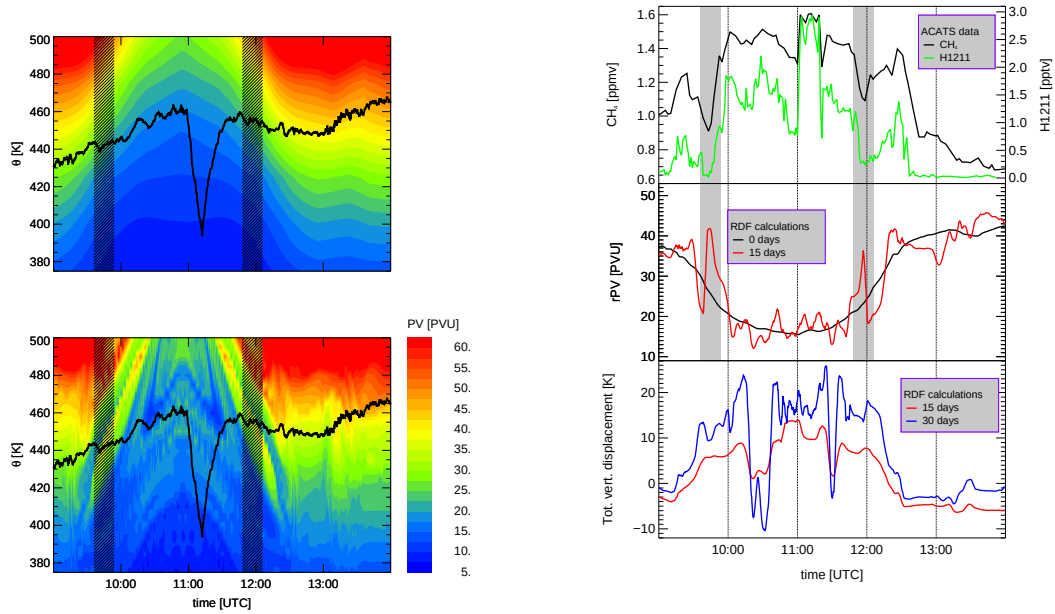

Figure 2. Top left: Potential vorticity (PV) derived from UKMO data shown as a vertical cross section of the vortex containing the ER-2 flight track on March 11, 2000. Bottom left: The same but with with the RDF PV (15 days) calculated by use of the 3d trajectories derived from isentropic UKMO winds and diabatic correction based on the *Morcrette* [1991] scheme. The time segments where filaments were observed are denoted as hatched regions. Top right: The observed CH_4 and Halon-1211 mixing ratios (ACATS). Middle right : Analyzed PV (black) and RDF-PV (red) along the flight track. Note that the RDF-PV fairly well reconstructs some of the observed tracer structures (hatched regions) and allows to interpret them as filaments of vortex air. Bottom right: The vertical displacement of the trajectories for 15 and 30 days RDF calculations. Positive (negative) values denote descent (ascent) of the air parcels. Values of $|\Delta\theta| < 20$ K justify the isentropic approximation used in CLaMS studies. All RDF time series are smoothed to remove the unphysical small-scale structures

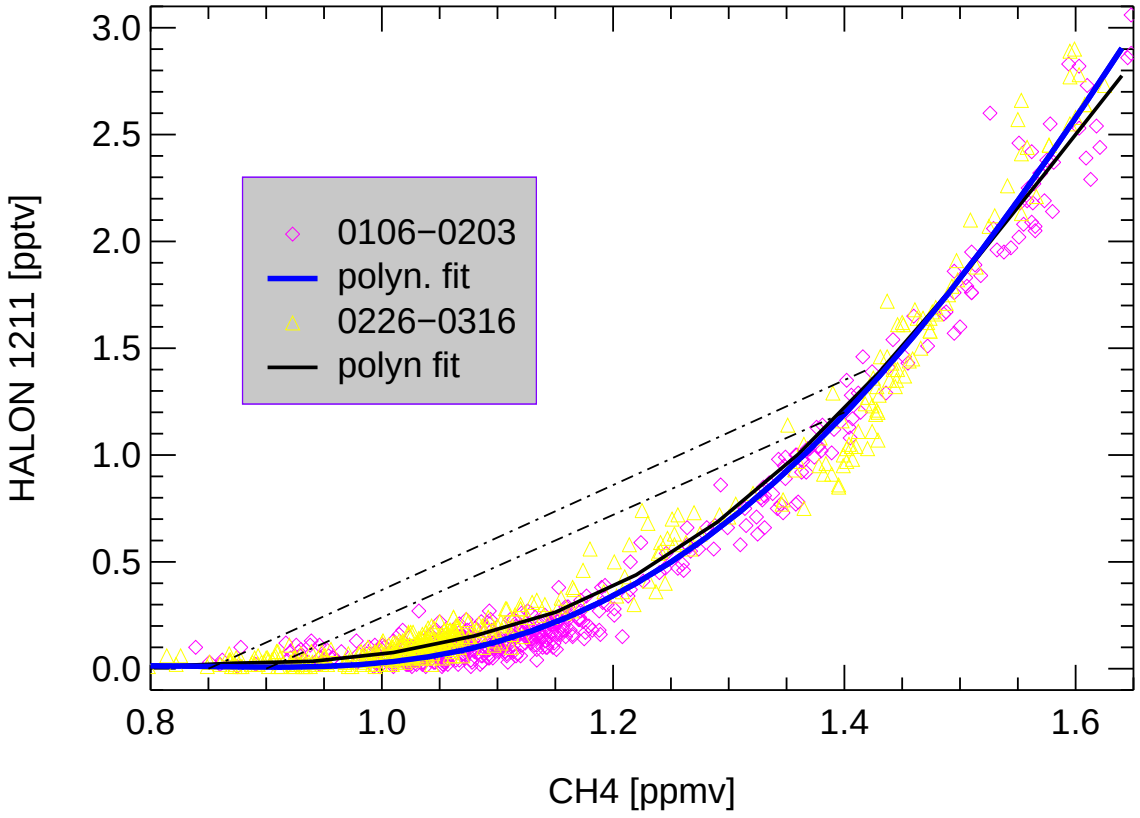

Figure 3. CH_4/Halon-1211 correlations (ACATS) derived from all ER-2 flights between January 6, and March 16 using polynomial fits (solid lines). The small difference between the blue (flights between 6.01 and 3.02, yellow triangles) and the black line (flights between 26.02 and 16.03, pink diamonds) indicates a weak influence of mixing on the Arctic stratosphere. Mixing events along the dashed lines (the so-called anomalous mixing [*Plumb et al.*, 2000]) were not observed during the considered period.

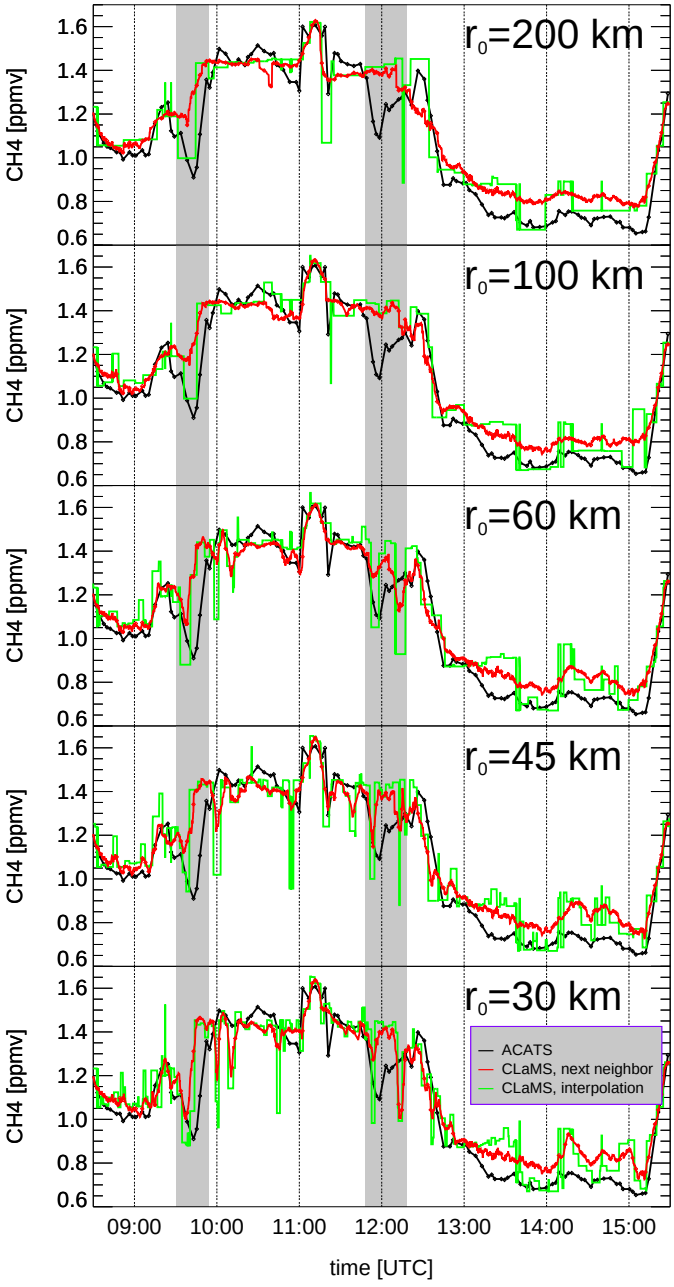

Figure 4. Pure advective transport of CH_4 (CLaMS without mixing) on March 11 for different model resolutions r_0. The trajectories are calculated from February, 10 to March 11, 12 UCT. Using for- or backward trajectories the (asynoptic) ER-2 flight is transformed to a synoptic time (March 11, 12 UCT). For comparison, the results of tracer transport are interpolated onto the synoptic ER-2 flight track either by taking into account only the nearest (green) or all the next neighbors (red).

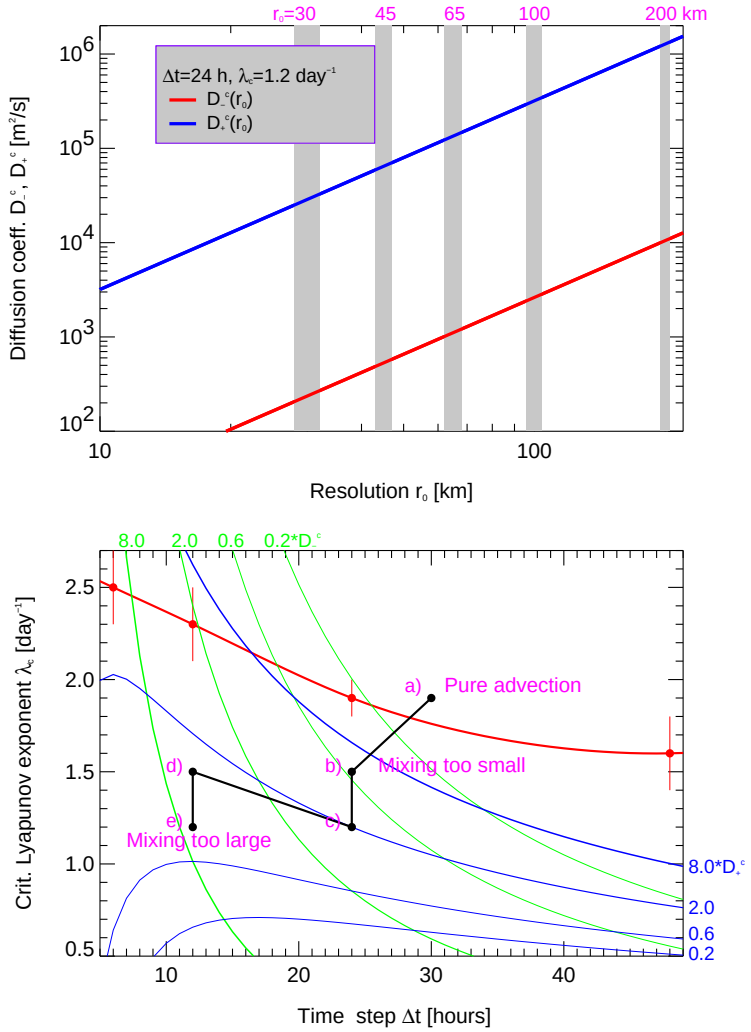

Figure 5. Dependence of the diffusion coefficients $D^c_\pm$ on the model parameters r_0, Δt and λ_c. Top: Assuming $\Delta t = 24$ hours and $\lambda_c = 1.2$ day^{-1}, $D^c_\pm$ is plotted versus r_0. The dashed regions denote CLaMS horizontal resolutions discussed in this paper together with their small variation due to the adaptive grid procedure. Bottom: This figure allows to estimate $D^c_\pm$ for arbitrary values in the $(\Delta t, \lambda_c)$ space. The relative values of D^c_+ and D^c_- (relative to $D^c_\pm(r_0)$ with $\Delta t = 24$ hours, and $\lambda_c = 1.2$ day^{-1}, see top panel) can be estimated from the blue and green isolines $\lambda_c = \lambda^\pm_c(\Delta t)$ (derived from (2)), respectively. The red points denote the maximal value of λ_c for a given time step Δt derived from isentropic ECMWF winds at $\theta = 450$ K during the considered time period. The polynomial spline (red) connects these points. Thus, $D^c_\pm = 0$ for $(\Delta t, \lambda_c)$ points lying above the red curve (pure advection). For two model resolution r_0 =45 and 100 km, we study the influence of mixing following the black path in the $(\Delta t, \lambda_c)$ space starting at point a) (no mixing), then moving to points b) (mixing too small), c), d), and finally reaching point e) (mixing too high). A significant increase of mixing along this path is caused by the increase of the lateral (effective) diffusivity D^c_-.

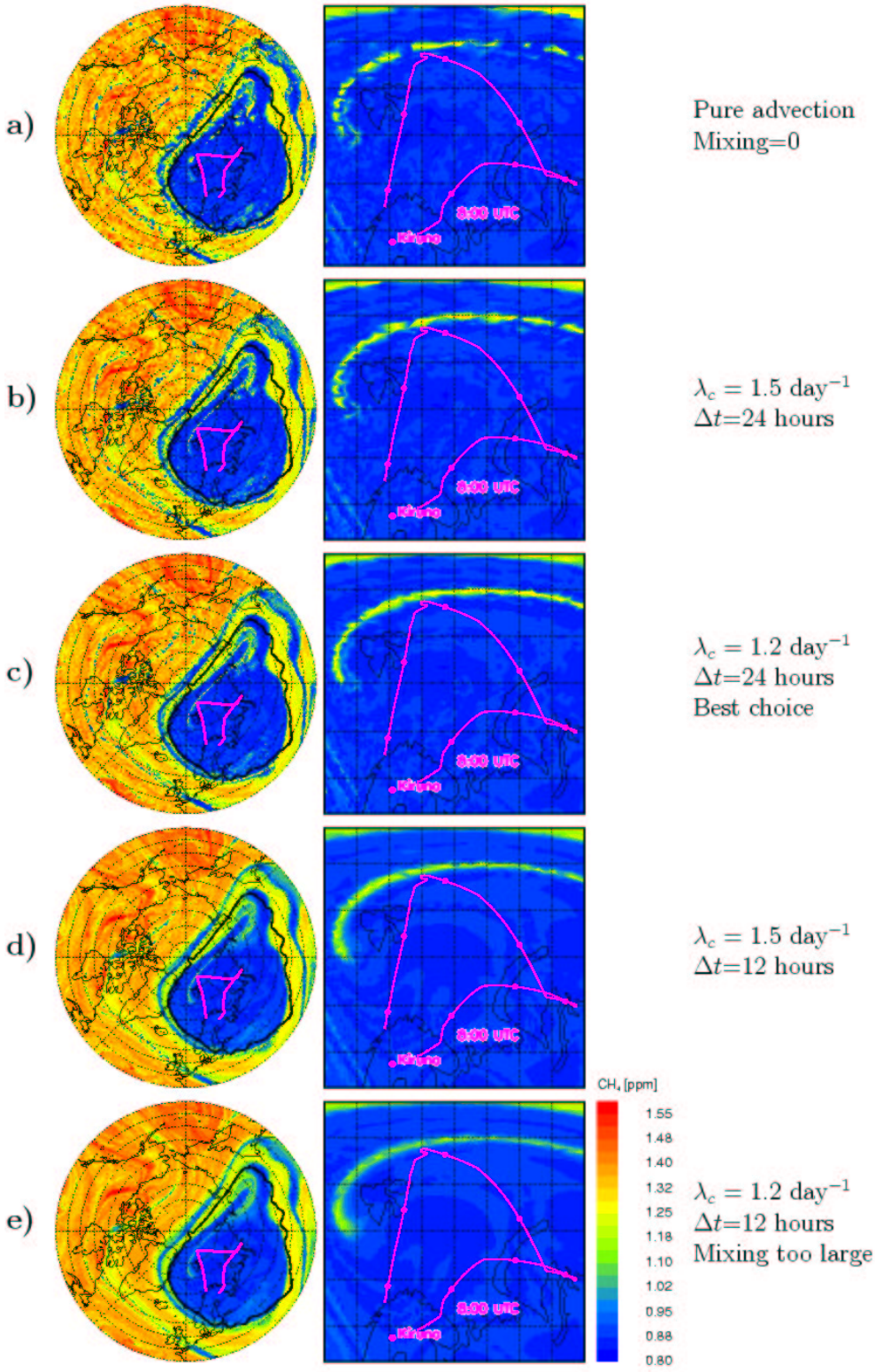

Figure 6. CLaMS distribution of CH_4 at $\theta = 450$ K on March 7, 2000, 12 UCT ($r_0 = 45$ km) together with the ER-2 flight transformed to a synoptic time. Left: Orthographic projection between 45 and 90 N. Right: The cylindric projection of a magnified section containing the ER-2 flight. The black line denotes the vortex edge identified by the strongest PV gradient with respect to the equivalent latitude [*Nash et al.*, 1996]

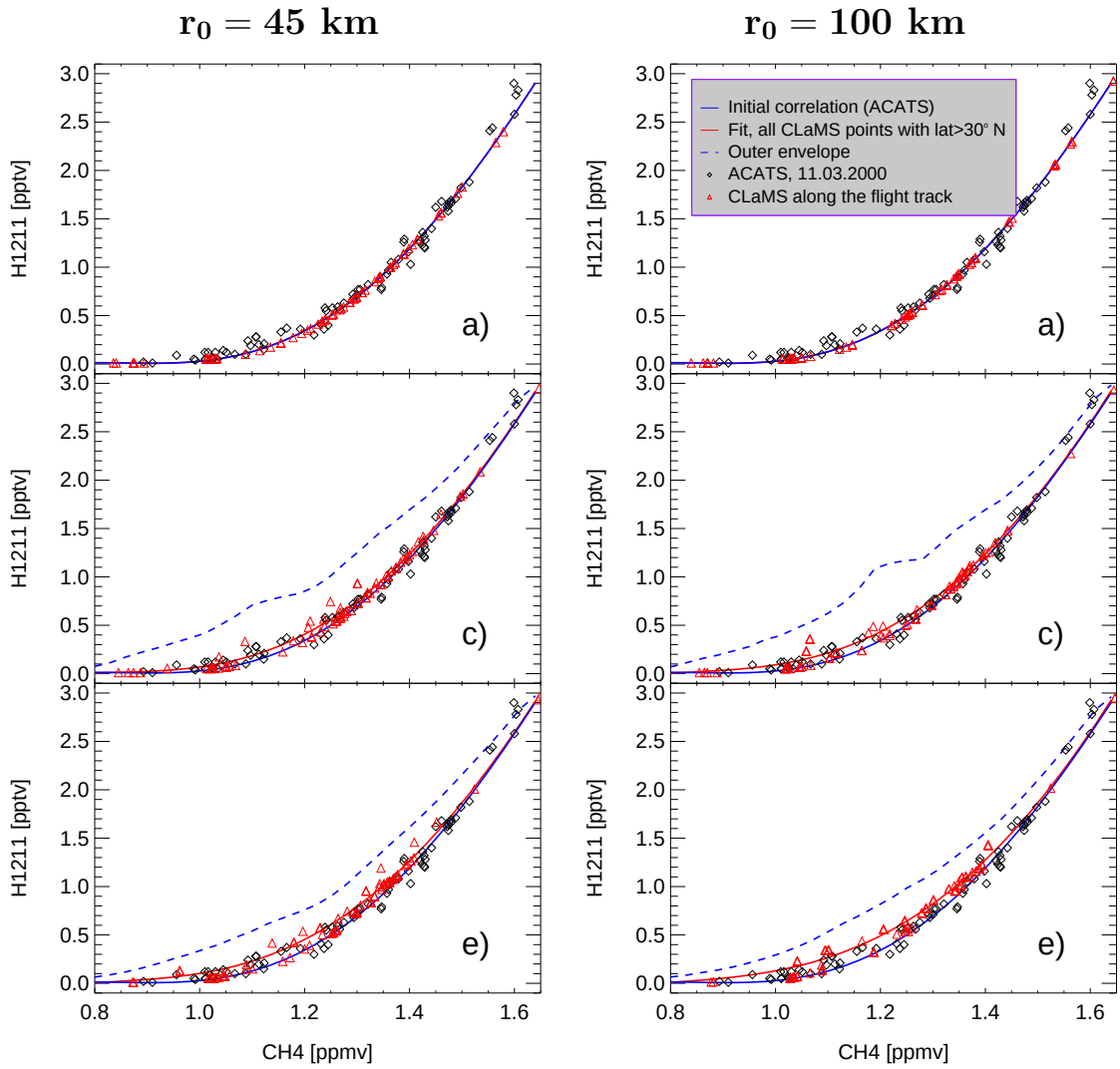

Figure 7. CLaMS CH_4/Halon-1211 correlations for March 11, 2000 derived for two different resolutions r_0 (left: 45 km, right: 100 km) and increasing mixing intensities changing from a) through c) to e) (see Fig. 5). The blue solid and dashed lines denote the outer (initial canonical correlation) and inner envelops of all CLaMS APs northward 30°N, respectively. A polynomial fit through these points is given by the red line. For comparison, the ACATS data obtained during the flight on March 11 (black diamonds) and the corresponding CLaMS results (red triangles) are shown.

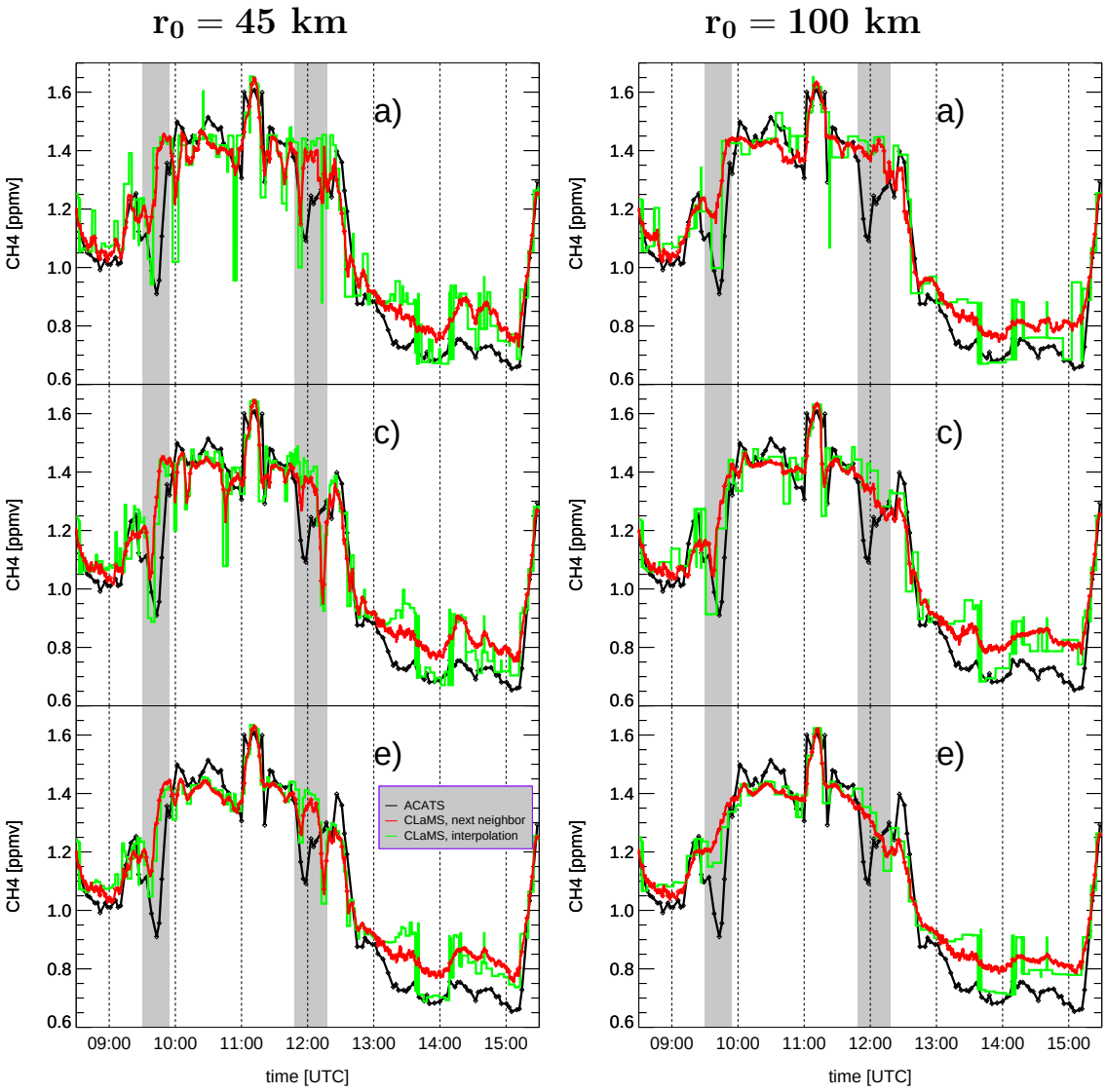

Figure 8. CLaMS versus ER-2 time series on March 11 derived for two different resolutions r_0 (left: 45 km, right: 100 km) and increasing mixing intensities changing from a) through c) to e). The observed values of CH_4 are transformed to a synoptic time (March 11, 12 UCT) by use of the isentropic trajectories. Two types of interpolation are used: either by taking into account only the nearest (green) or all the next CLaMS neighbors (weighted interpolation, red).

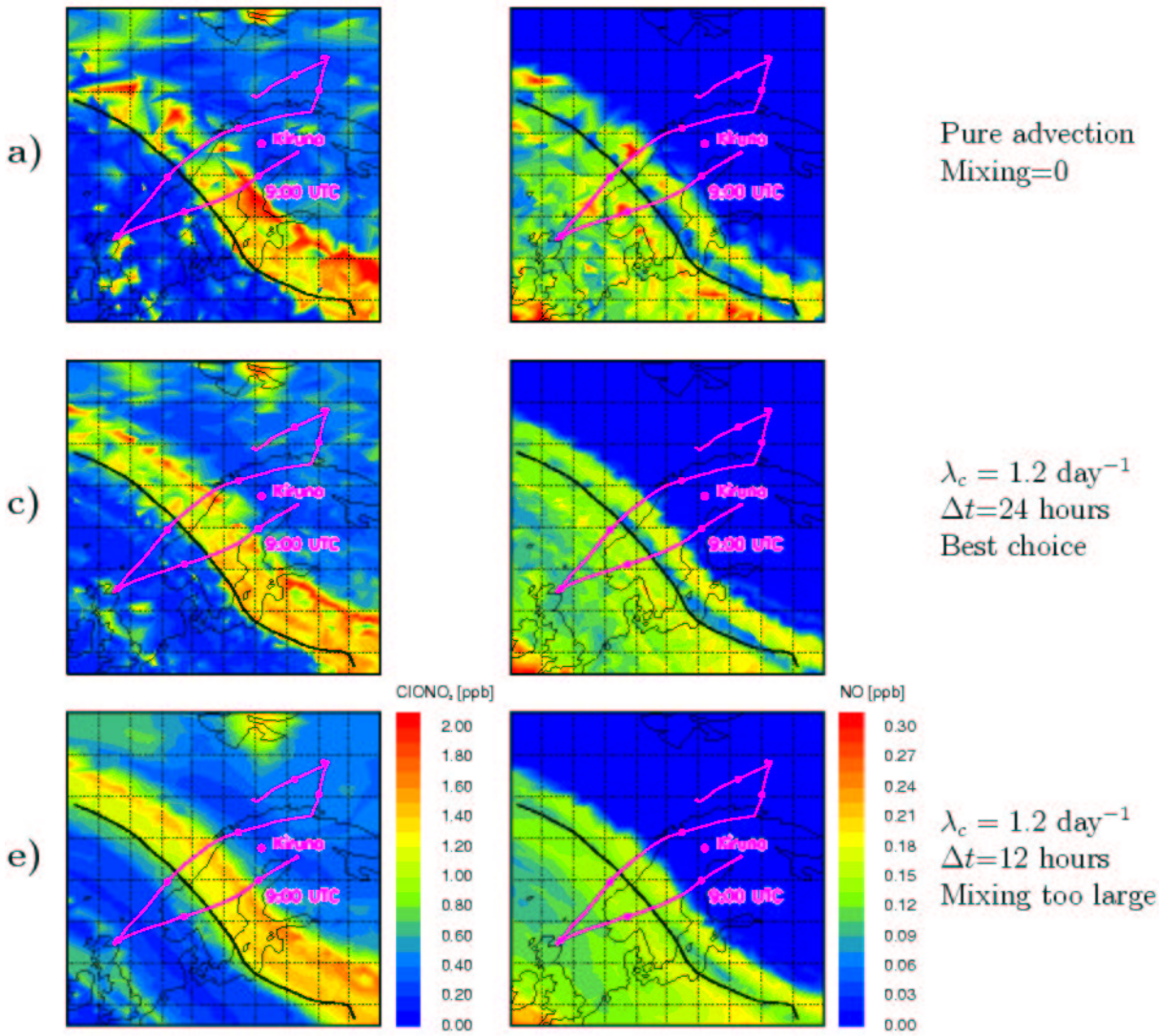

Figure 9. Influence of an increasing mixing intensity in the model (from top to bottom) on the formation of $ClONO_2$ (left) and on the NO distribution (right) on March 11 at the edge of the polar vortex over Scandinavia at $\theta = 450$ K. The black line denotes the edge of the polar vortex identified by the strongest PV gradient with respect to the equivalent latitude [*Nash et al.*, 1996].

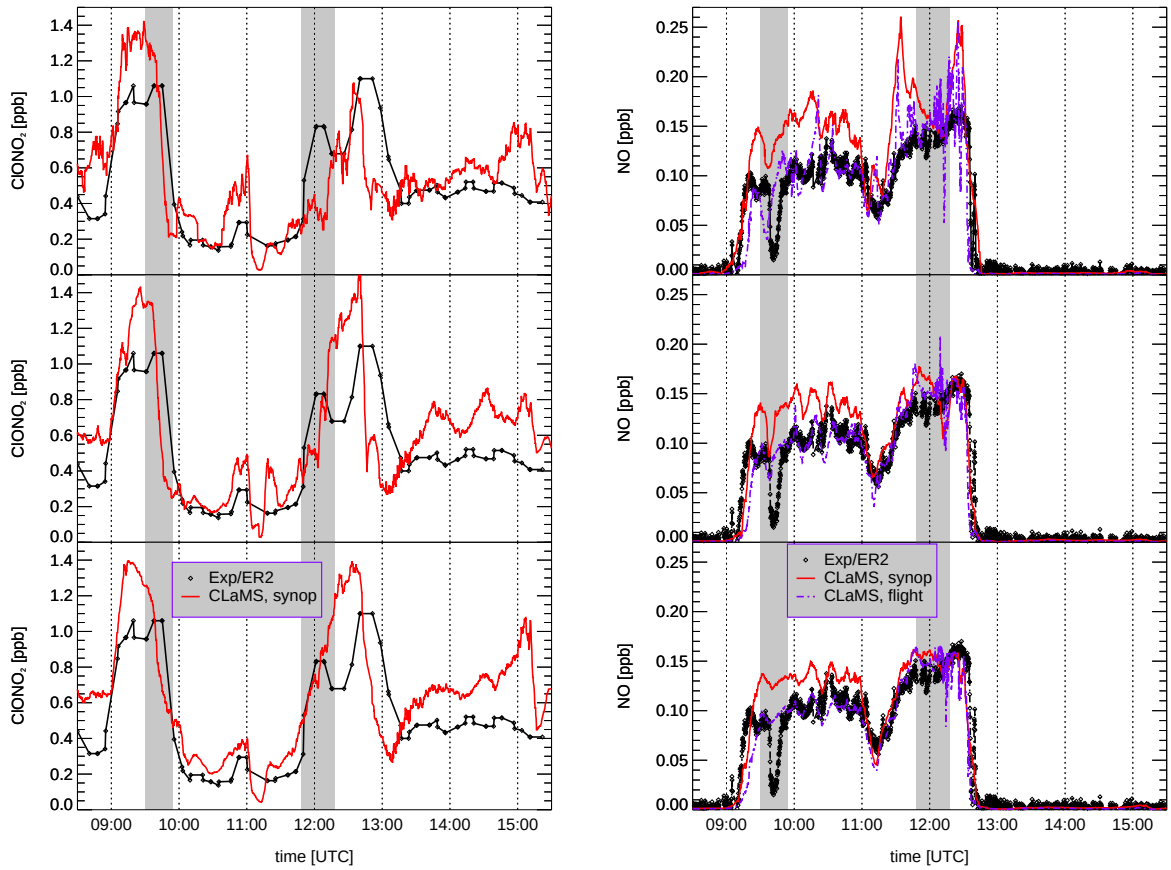

Figure 10. Sensitivity of the simulated $ClONO_2$ (left) and NO (right) time series with respect to mixing (top: pure advection, middle: best choice, bottom: mixing too high) The black diamonds denote the measured mixing ratios. The red curve describes interpolated CLaMS values along the synoptic track (weighted interpolation, see Fig. 8). The violet curve additionally takes into account the diurnal variations of NO. Within the hatched time segments the vortex edge was crossed.

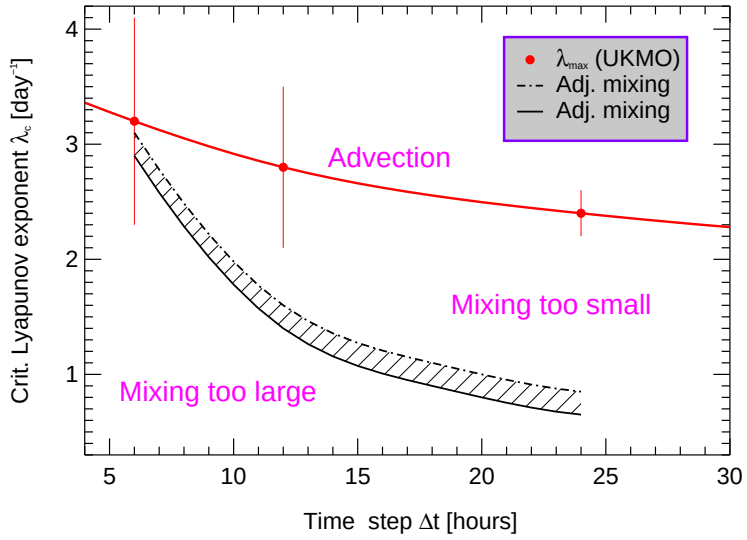

Figure 11. The dashed area denotes the $(\Delta t, \lambda_c)$ where best agreement with experimental data was achieved for spatial resolutions $r_0 = 45$ km (solid) and 100 km (dashed). The maximal values of λ_c for a given time step Δt derived from isentropic ECMWF winds at $\theta = 450K$ during the considered time period are shown by the red line. Thus, choosing $(\Delta t, \lambda_c)$ values above this curve, the transport is reduced to a pure advection.

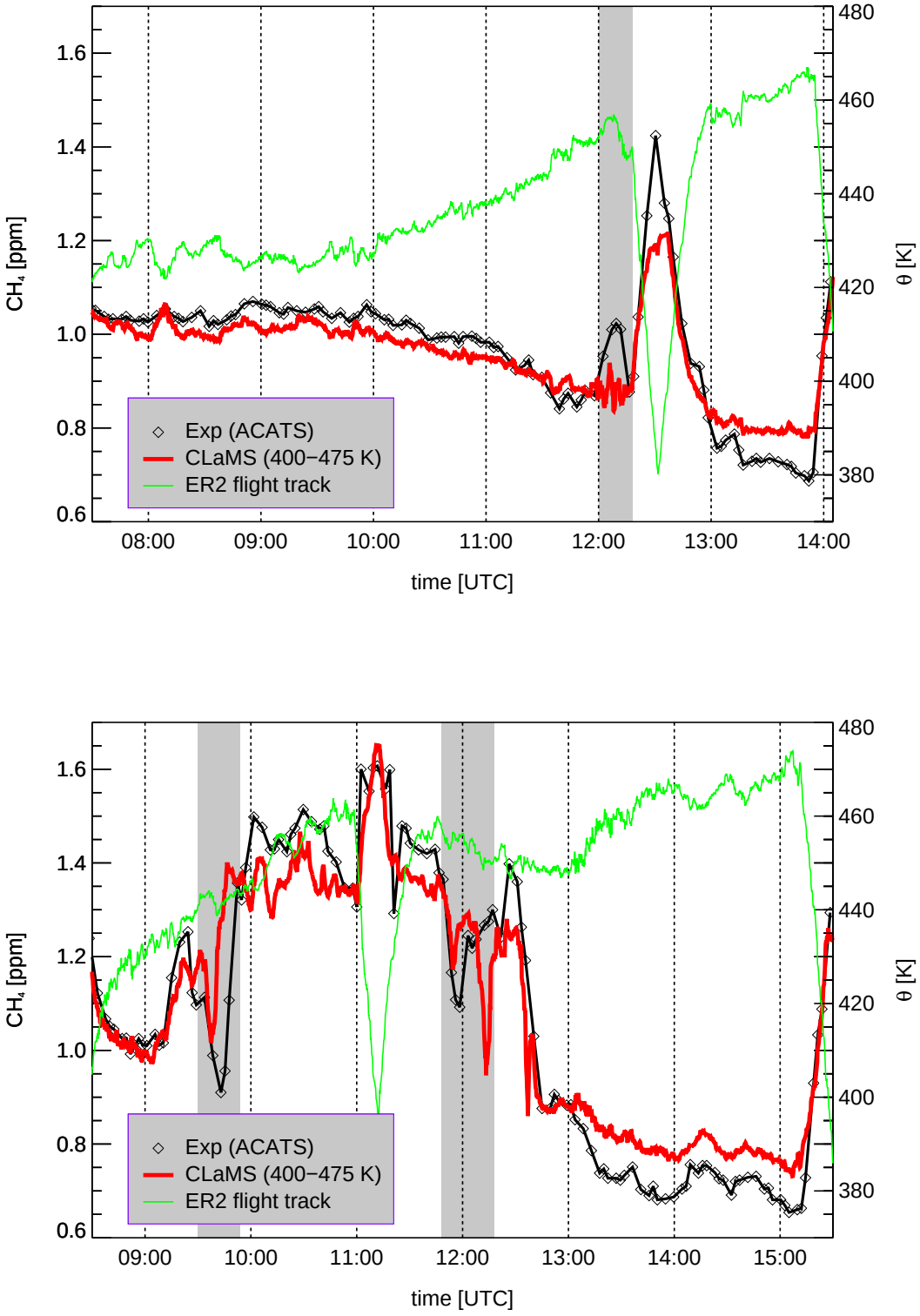

Figure 12. CLaMS results with $r_0 = 45$ km and optimized mixing for March 7 (top) and 11 (bottom) compared with experimental data. The hatched areas denotes regions were filaments were encountered.

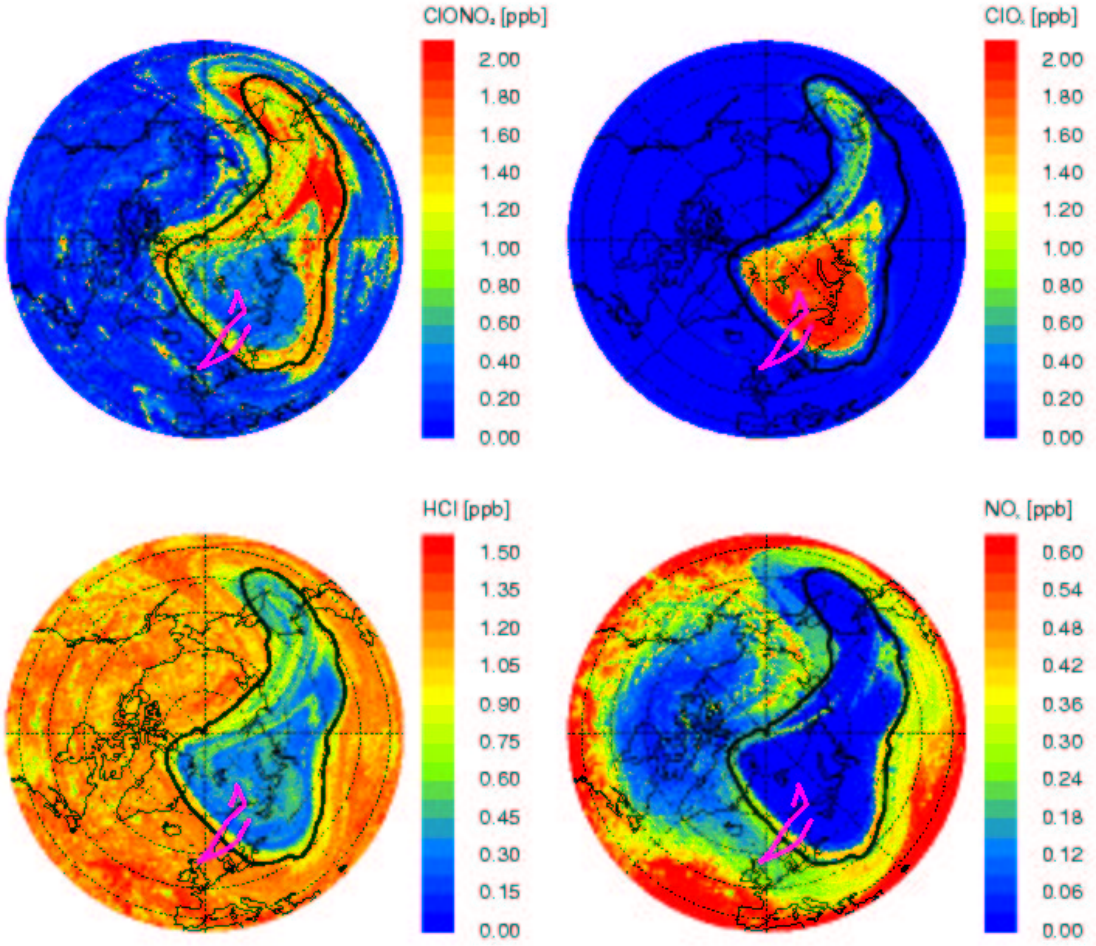

Figure 13. Formation of $ClONO_2$-collar on March 11 together with the vortex edge identified by the strongest PV gradient with respect to the equivalent latitude [*Nash et al.*, 1996]. Top left: The $ClONO_2$-collar is defined by its inner and outer edges. Top right: Enhanced ClO_x mixing ratios in the interior of the vortex are only possible due to strong denoxification (i.e. transformation of NO_x to HNO_3) of the vortex core and the presence of PSCs re-activating the fresh formed $ClONO_2$. This area defines fairly well the inner edge of the $ClONO_2$-collar. Bottom left: Strong decrease of HCl within the vortex defines the region of chlorine activation and the outer range of the $ClONO_2$-collar. Bottom right: The small NO_x-values within the vortex are caused either by the denoxification (vortex core) or by the deactivation ($ClONO_2$-collar).

Tables

Table 1. Spatial variability of the simulated CH_4 time series f_s (nearest neighbor approximation) for CLaMS studies without and with mixing compared with the experimental data f_{exp} containing n data points. Here the ratio $\gamma = \Delta_s/\Delta_{exp}$ is determined with $\Delta_l = \sum_{i=1}^{n} |f_l(t_{i+1}) - f_l(t_i)|$ and $l = s, exp$.

CLaMS without mixing		CLaMS with mixing		
Resolution (km)	γ	Case	γ, (r_0=45 km)	γ, (r_0=100 km)
200	0.78	a)	1.78	0.89
100	0.89	b)	1.48	1.10
60	1.27	c)	1.06	0.89
45	1.78	d)	0.93	0.64
30	1.92	e)	0.82	0.60

Table 2. Mixing intensity in terms of the lateral effective diffusivity $D^c_{\_}$ calculated for different resolutions r_0 and different values of Δt and λ_c along the black path in Fig. 5.

Case	Δt [h]	λ_c [d^{-1}]	$D^c_{\_}$ [$m^2 s^{-1}$] r_0=45 km	$D^c_{\_}$ [$m^2 s^{-1}$] r_0=100 km
a)	24	∞	0.0	0.0
b)	24	1.5	2.9×10^2	1.4×10^3
c)	24	1.2	5.3×10^2	2.6×10^3
d)	12	1.5	2.6×10^3	1.3×10^4
e)	12	1.2	3.5×10^3	1.7×10^4